



Thermo-compositional structure of the north-eastern Canadian Shield from Rayleigh wave dispersion analysis as a record of its tectonic history

Isabella Altoe^{a,*}, Thomas Eeken^a, Saskia Goes^a, Anna Foster^b, Fiona Darbyshire^c

^a Department of Earth Science and Engineering, Imperial College London, UK

^b School of Earth Science Energy and Environment, Yachay Tech University, Urcuquí, Ecuador

^c Centre de recherche GEOTOP, Université du Québec à Montréal, Montreal, Quebec, Canada

ARTICLE INFO

Article history:

Received 13 December 2019

Received in revised form 4 June 2020

Accepted 6 July 2020

Available online 22 July 2020

Editor: R. Bendick

Keywords:

lithosphere
geotherm
metasomatic alteration
Superior Craton
Grenville
Mid-Continent Rift

ABSTRACT

The thermal and compositional structure of lithospheric keels underlying cratons, which are stable continental cores formed during the Precambrian, is still an enigma. Mapping lithospheric temperatures and compositional heterogeneities is essential to better understand geodynamic processes that control craton formation and evolution. Here we investigate the northeastern part of North America which comprises the Superior Craton, the largest Archean craton in the world, and surrounding Proterozoic belts. We model Rayleigh-wave dispersion curves from a previous study, which were regionalised based on cluster analysis. Next, we perform a grid search for sub-crustal thermal and compositional structures that are consistent with the average dispersion curve for each cluster. We apply constraints on crustal structure and use thermodynamic methods to map thermo-compositional structures into seismic velocity. In agreement with previous studies, most regions require concentrations of metasomatic minerals over certain depth intervals to fit the seismic profiles. Our results further require vertical as well as lateral variations in compositional and thermal structures, which appear to reflect different stages of formation and modification of the lithosphere below the region, with distinct structures found under Archean cores, Archean/Paleoproterozoic collision belts, mid-late Proterozoic collision belts, and zones affected by rifting.

© 2020 Elsevier B.V. All rights reserved.

1. Introduction

1.1. Overview

Old continental cores have been stable for a long time, but it is still debated how these cores formed and survived for billions of years (e.g., van Hunen and Moyen, 2012; Lee et al., 2011; Sleep, 2005). End-member mechanisms are (a) formation by extensive melting in plumes in a hotter Archean mantle, which would have left thick residues of relatively depleted and thereby buoyant and strong dry mantle lithosphere, or (b) formation by lateral accretion in a subduction environment, which may have differed from today's subduction as a hotter mantle would have made plates more buoyant with thicker magmatic crust and thicker depleted dry lithosphere.

From the geologic record, it is clear that, before reaching the tectonically quiet stage that they have experienced for the past

hundreds of millions of years to over a Gyr, continental cores have seen a long tectonic history with evidence of several generations of deformation and magmatism. Indeed, where detailed images of crustal structure are available (e.g. the Canadian Lithoprobe project; Clowes, 2010), they reflect the complexity expected from the surface record. By contrast, cratonic mantle lithosphere is often treated as geophysically relatively homogeneous, with a composition inferred from averaging compositions found in mantle xenoliths (e.g. Jordan, 1978; Griffin et al., 2009), assumed to be in thermal equilibrium, and with little variation in heat flow at the Moho (Mareschal and Jaupart, 2004; Cooper et al., 2004). Most compositional complexity inferred from the xenolith record (O'Reilly and Griffin, 2010) involves peridotites with different degrees of depletion or refertilisation in basaltic components, which seismically are difficult to distinguish (e.g. Schutt and Lesher, 2006).

However, recent studies have found discontinuities within cratonic keels indicating both sudden increases and (more surprising) decreases in seismic velocities with depth (e.g., Miller and Eaton, 2010; Abt et al., 2010). Furthermore, several tomographic studies of bulk P and S velocities find more pronounced seismic heterogeneity than can be explained with varying amounts of lherzo-

* Corresponding author.

E-mail address: i.altoe17@imperial.ac.uk (I. Altoe).

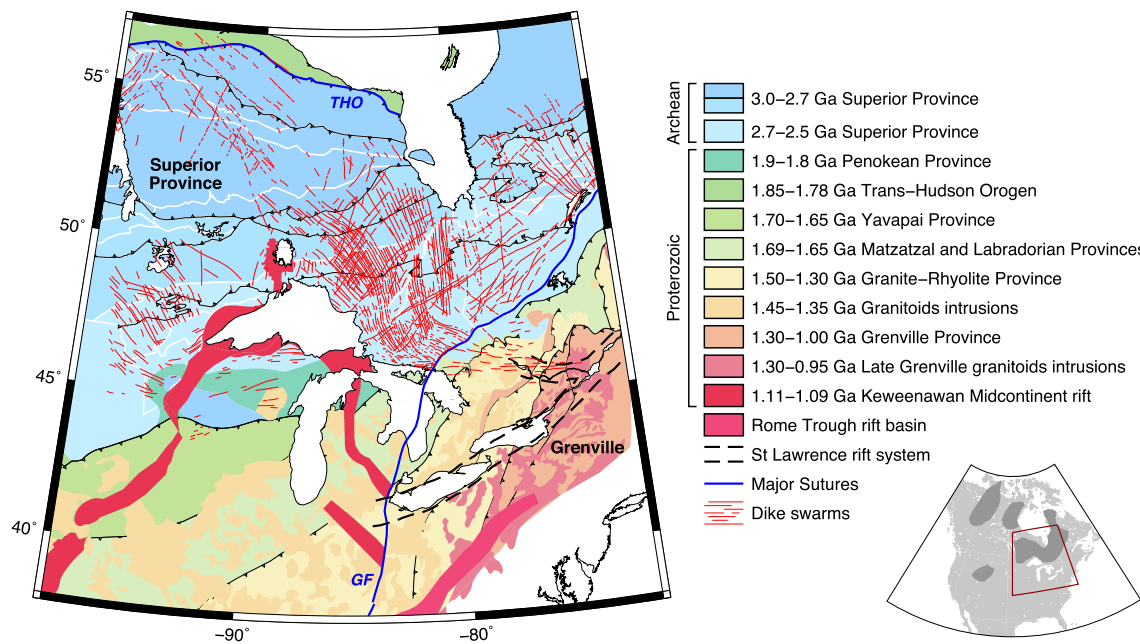


Fig. 1. Simplified tectonic map of the Eastern North American Craton (adapted from Whitmeyer and Karlstrom, 2007). The subprovinces of the Superior Province are outlined in white, and its main thrust faults in black (adapted from Percival et al., 2012; Clowes, 2010). In red are the main diabase dyke swarms of the Canadian Shield (adapted from Buchan and Ernst, 2004). The dashed black lines are the extension of the St. Lawrence rift zone (adapted from Boyce and Morris, 2002), and the full blue lines are the major sutures: (THO) Trans Hudson Orogen, and (GF) Grenville Front. (For interpretation of the colours in the figure(s), the reader is referred to the web version of this article.)

lites, harzburgites and dunites (e.g. Bruneton et al., 2004; Hieronymus and Goes, 2010; Eeken et al., 2018). It has been suggested that metasomatic alteration forming either low-velocity hydrated or carbonated minerals, or high-velocity diamonds (Selway et al., 2014; Eeken et al., 2018; Garber et al., 2018) may have a more significant effect on large-scale geophysical structure, both in terms of density and seismic velocity, than previously thought.

In a previous study, we developed a method to interpret 1-D phase-velocity dispersion curves in terms of temperature and composition (Eeken et al., 2018). Recently (Eeken et al., 2020), we adapted this method for 3D structure and applied it to Rayleigh-wave phase velocities from a study by Petrescu et al. (2017) that covered the easternmost part of the Archean Superior Province and the adjacent Proterozoic Grenville Province.

We found systematic differences in composition between the Superior and Grenville, with the latter on average containing more metasomatic alteration of the shallow mantle lithosphere, in particular below regions with a record of extensive arc volcanism. In addition, the phase-velocity data required variations in thermal structure, with an overall north to south warming/thinning of the lithosphere below the study region. In the current paper, we apply this method to a region adjacent to that studied by Eeken et al. (2020), using phase velocities from a new tomographic model by Foster et al. (2020). Our study area is significantly larger and comprises a wider range of tectonic domains, including a much larger part of the Superior craton, part of the Trans-Hudson Orogen, much of the Mid-Continent Rift, parts of the Grenville, and several Proterozoic terranes south of the Superior. The results reveal variations in seismic and associated compositional structure that appear to reflect tectonic history.

1.2. Tectonic background

The North American Craton was formed by amalgamation of several Archean cratons (Slave, Rae-Hearne, Superior, and Wyoming as well as some smaller continental fragments) during the Paleoproterozoic (2.0–1.8 Ga) (Hoffman, 1988; Whitmeyer and

Karlstrom, 2007). The Superior Province is often regarded as the Archean core of the North American Craton. This province consists of mostly east-west trending metasedimentary terranes, metaigneous volcanic and plutonic complexes, and granite-greenstone belts (Fig. 1). These terranes were assembled by progressive accretion around the North Caribou Superterrane (Thurston, 1991). The Superior Province has been tectonically stable since 2.6 Ga and it is bounded by Proterozoic orogenic belts (Percival et al., 2012).

The Trans-Hudson orogenic (THO) belt (1.85 - 1.78 Ga), to the north and west of the Superior Province, was the result of the collision between the Rae-Hearne, Wyoming and Superior cratons to form the cratonic core of Laurentia (Hoffman, 1988). Concomitant to the THO, the Penokean orogeny (1.87 - 1.83 Ga) metamorphosed Archean basement and Paleoproterozoic supracrustal rocks of the Superior Craton at the southern margin of Laurentia (Hoffman, 1988). Following this assembly stage, for a period of 800 Ma, several further provinces were added by arc-continent accretion (Hoffman, 1988; Whitmeyer and Karlstrom, 2007). The main provinces are the Yavapai Province (1.70 - 1.65 Ga, added to the south), the Matzatzal and Labradorian Provinces (to the south and northeast, respectively; 1.69 - 1.65 Ga), the Granite-Rhyolite Province (to the south, 1.50 - 1.30 Ga) and the Grenville Province (to the east, 1.30 - 1.0 Ga) added during the Grenville orogeny (1.30 - 0.95 Ga). The Grenville orogeny, a continent-continent collision, was part of the formation of Rodinia, deforming and reworking some of the juvenile provinces and the Superior Province at the eastern margin of Laurentia. These episodes of accretion were associated with events of granitoid plutonism which stitched new and older terranes (Hoffman, 1988).

During its geological history, the study region was affected by plume activity as well as rifting events. Igneous activity associated with plumes dates back to the Archean and can be identified by mafic dyke swarms (Ernst and Bleeker, 2010). In addition, the region was affected by the Keweenawan Mid-Continent Rift (1.11 - 1.09 Ga), which resulted in one of the world's largest flood basalt provinces (by volume). The rift system also includes the Nipigon Embayment, in the area of Lake Nipigon north of Lake Superior;

which is related to the early stages of rifting, and is believed to have acted as a failed arm during the Keweenawan event (Heaman et al., 2007).

More recently, with the break up of the Rodinia supercontinent (0.62 - 0.57 Ga), an interior rift system was formed in eastern North America associated with the opening of the Iapetus Ocean (Thomas, 1991). Also related to this event, the St. Lawrence rift was formed and it is thought that the main system of northeast-southwest-trending faults from this rift extends to the lower Great Lakes (Boyce and Morris, 2002).

1.3. Previous studies of lithospheric structure

The crust and uppermost mantle beneath the eastern North American Craton have been widely studied using several methods. The most extensive effort, the Canadian Lithoprobe Project (imaging as deep as 120 km) (Hammer et al., 2010), was a multidisciplinary research programme that used seismic reflection and refraction data combined with other geological, geochemical and geophysical methods to study 10 transects across Canada. Our study area includes the following transects: the Western Superior (e.g., Percival et al., 2006; Musacchio et al., 2004), the Great Lakes (e.g., Cannon et al., 1991; Shay and Tréhu, 1993), the Kapskasing Structural Zone and the Abitibi-Grenville (e.g., Winardhi and Mereu, 1997; White et al., 2000). They found evidence of ancient suture zones within the Superior and Grenville Provinces. In the Superior Province, northward-dipping crustal reflections were found penetrating the Moho and extending into the mantle lithosphere. This fabric is consistent with sequential subduction and accretion from the south and was interpreted as preserved subduction thrusts. The main examples are dipping crustal reflectivity beneath the Abitibi subprovince in the southeastern Superior (Calvert et al., 1995), and a dipping sub-Moho reflector beneath the southwestern Superior Province (Musacchio et al., 2004). In the Grenville Province, southeast dipping thrust structures were imaged associated with the deformation front, extending into the middle and lower crust (White et al., 2000).

More recently, studies using receiver function analysis, surface-wave and body-wave data (including Darbyshire et al., 2007; Petrescu et al., 2016; Eaton et al., 2006; Thompson et al., 2015; Chen and Li, 2012; Li et al., 2003) contributed further information on crustal and mantle structure. Petrescu et al. (2017) and Boyce et al. (2016) found that the region is characterised by faster upper mantle beneath Archean terranes than beneath Proterozoic belts, which was interpreted as due to metasomatism of the Proterozoic lithosphere. P-wave tomographic models of the Superior Province by Bollmann et al. (2019), Frederiksen et al. (2013), and Frederiksen et al. (2007) show a high-velocity anomaly beneath the western Superior Province and a low-velocity anomaly beneath the eastern Superior. Other features include low-velocity anomalies associated with the Mid-Continent Rift and its northwards extension under the Nipigon Embayment. Low-velocity anomalies have also been observed underlying the Grenville Province near the lower Great Lakes by Chen and Li (2012) and Li et al. (2003) and were associated with the Great Meteor hotspot (100 - 120 Ma). A recent P-wave tomographic study revealed north-south variations in the structure below the Grenville orogen, attributed to more extensive metasomatic alteration south than north of the Great Lakes (Boyce et al., 2019).

In the Hudson Bay area, Gilligan et al. (2016) performed a joint receiver function-dispersion data inversion for crustal and upper mantle structure, while Miller and Eaton (2010) and Darbyshire et al. (2013) used receiver functions and surface waves, respectively, to investigate lithosphere architecture across Hudson Bay. Although they found no clear correlation between crustal age and lithospheric thickness, the lithospheric thickness seems to vary

greatly across the region and there are signs of lithospheric layering (Darbyshire et al., 2013). Using S-wave receiver functions, Miller and Eaton (2010) imaged high-velocity lithospheric discontinuities dipping beneath the Canadian Shield, that they interpreted as remnant slabs that were accreted during the Trans Hudson Orogeny. Porritt et al. (2015) used S-to-P receiver function and teleseismic phase velocities to infer that the lithosphere is thicker beneath Hudson Bay (~350 km), and thinner around the periphery of the Bay (~200-250 km). Within the lithosphere, they imaged mid-lithospheric discontinuities at ~80-120 km depth, which were attributed to trapped terranes and shear zones around the cratons. The Mid-Continent Rift was also extensively studied by Zhang et al. (2016) as part of the Superior Province Rifting Earthscope Experiment (SPREE). The study identified a transitional layer along the Mid-Continent Rift interpreted as evidence of extensive underplating.

Heat flow and heat production data have been used to estimate the relative contributions of crustal heat production and mantle heat flow to the thermal state of the lithosphere. Jaupart et al. (1998), Mareschal and Jaupart (2004), and Perry et al. (2006a) inferred that crustal heat production was the dominant control on variations in surface heat flow in the stable Canadian Shield. However, a study by Lévy and Jaupart (2011) combining heat flow and teleseismic travel times concluded that the travel-time delays could not be explained by variations in crustal heat production alone, and also required variations of heat supply from below the crust. Deep heat flow variations are attributed to lithospheric thickness variations as large as 80 km across the region.

Studies of kimberlite mantle xenoliths and xenocrysts have been used to understand the composition and history of the Superior Province lithospheric mantle. Major and trace element analysis of garnet xenocrysts in Paleozoic and Mesozoic kimberlites indicate a depleted shallow mantle, increasing in fertility with depth (Scully et al., 2004), but this trend with depth was not observed in older 1.1-Ga kimberlites. The change was interpreted as evidence of modification of the lithospheric mantle by igneous activity related to the Mid-Continent Rift formation (Scully et al., 2004). This study also suggests that the extent of lithospheric modification varies spatially, based on differences in garnet chemistry between adjacent kimberlite pipes.

2. Data and method

To estimate the upper mantle thermo-chemical structure of the eastern part of the North American Craton we used Rayleigh-wave phase-velocity dispersion curves from Foster et al. (2020). The dispersion curves were grouped by cluster analysis and the groups further subdivided based on crustal structure. To match the average dispersion curve of each group, we performed a grid-search of forward models calculated for a large set of possible combinations of compositions and lithospheric geotherms.

2.1. Dispersion data and regionalisation by cluster analysis

The data used in this study consist of a set of 1D Rayleigh-wave dispersion curves extracted from phase-velocity maps (Foster et al., 2020) (Fig. 2). The phase-velocity maps were derived using a tomographic inversion of dispersion curves measured using a two-station cross-correlation method. The inversion solves both for isotropic phase-velocity variations and azimuthal anisotropy; in this study, we use the isotropic phase component for the period range of 20-160 s. Foster et al. (2020) discuss interpretation of the anisotropic structure. From the original study, we selected an area with a good amplitude recovery based on resolution tests and grid points with a minimum azimuthal coverage of 65% per period (Fig. 3).

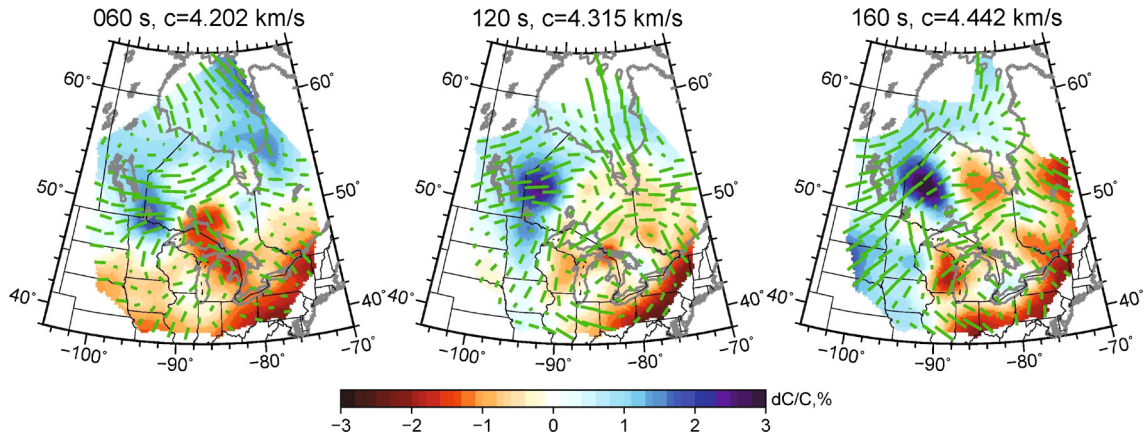


Fig. 2. Rayleigh-wave phase-velocity maps at selected periods, from inversion of two-station dispersion measurements from Foster et al. (2020). C is the regional average velocity for that period. The green bars show the orientation and magnitude of azimuthal anisotropy.

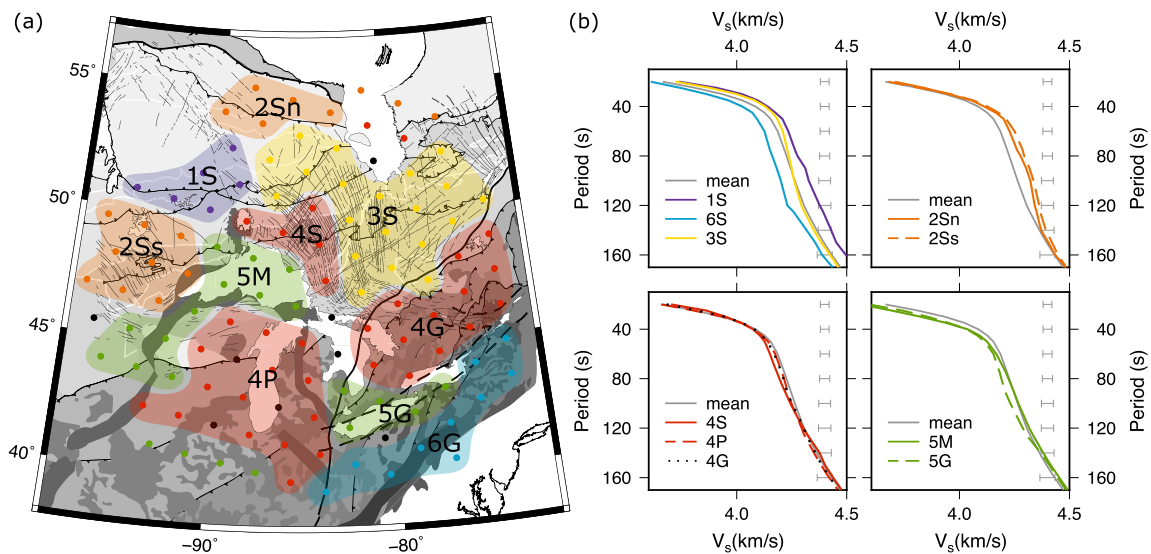


Fig. 3. (a) Map showing the grid nodes of the phase-velocity map (from Foster et al. (2020)) with the final regionalisation based on the cluster analysis (represented by the different colours and numbers), and further division into groups based on crustal structure (S - Superior Province, M - Mid-Continent rift, P - Proterozoic crust, G - Grenville). The final groups are: 1S (western Superior), 2Sn (northwestern Superior), 2Ss (southwestern Superior), 3S (eastern Superior), 4S (southern Superior), 4P (Proterozoic crust), 4G (Grenville), 5M (Mid-Continent Rift), 5G (Grenville - St. Lawrence Rift), and 6G (eastern Grenville). Points with a negative silhouette value (in black), and points not assigned to any group were not included in our subsequent modelling. (b) Average dispersion curve for each group compared with the average dispersion curve for all groups (grey curve). Error bars on the right of the dispersion curves are the period-dependent uncertainties that were used in the subsequent thermo-chemical modelling.

Given the resolution and sensitivity of the data, modelling each individual grid node is not a reasonable approach since they are not independent. Therefore, we used cluster analysis to identify regions with distinct structure. In particular, we applied the k-means algorithm (Hartigan and Wong, 1979; Hartigan, 1975) and used the measures of spread within and between the clusters and the silhouette value (Rousseeuw, 1987; Kaufman and Rousseeuw, 1990) to select the optimal number of clusters. Based on those quality tests, we identified six as the optimum number (also see Supplementary Section S1). Additionally, this division clearly correlates with the tectonics of the region, which gives us confidence that the groups actually represent the main variations in the lithospheric structure (Fig. 3(a)).

Although the six clusters appear to characterise regions of similar upper mantle structure, literature identifies significant crustal variation within some of the clusters, in particular where the cluster covers several spatially separated regions. Because the short periods of the Rayleigh waves are sensitive to the crustal structure, those velocity variations affect the modelling. Therefore, the six clusters were further subdivided into ten groups (Fig. 3).

Groups 2Sn and 2Ss cover the northern and southern borders of the western Superior Province. Groups 1S and 3S cover the western and eastern core of the Superior. Group 4S covers the region where the Superior borders the Mid-Continent Rift, including the Nipigon Embayment. Group 5M follows the Mid-Continent Rift and 5G the St. Lawrence-Southern Great Lakes rift structures. Region 4P covers the Proterozoic terranes that accreted to the south of the Superior, and 4G and 6G cover distinct parts of the Grenville Orogen.

When comparing the average dispersion curve of each group it is notable that the dispersion curves from different clusters have distinct shapes (Fig. 3(b)). Group 1S, in the central-western Superior, is overall the fastest, and group 6G in the southernmost part of the Grenville, is overall the slowest. Groups 4S, 4G, and 4P, which fall in three different tectonic regions, have slightly lower velocities at shorter periods than the eastern Superior region 3S. The dispersion curves for groups 2Sn and 2Ss have a distinct shape with higher velocities at shorter to intermediate periods, decreasing in velocity at longer periods. Lastly, groups 5G and 5M are characterised by slow velocities at shorter to intermediate periods. Uncertainties were assigned to each curve (Fig. 3(b)) based on the

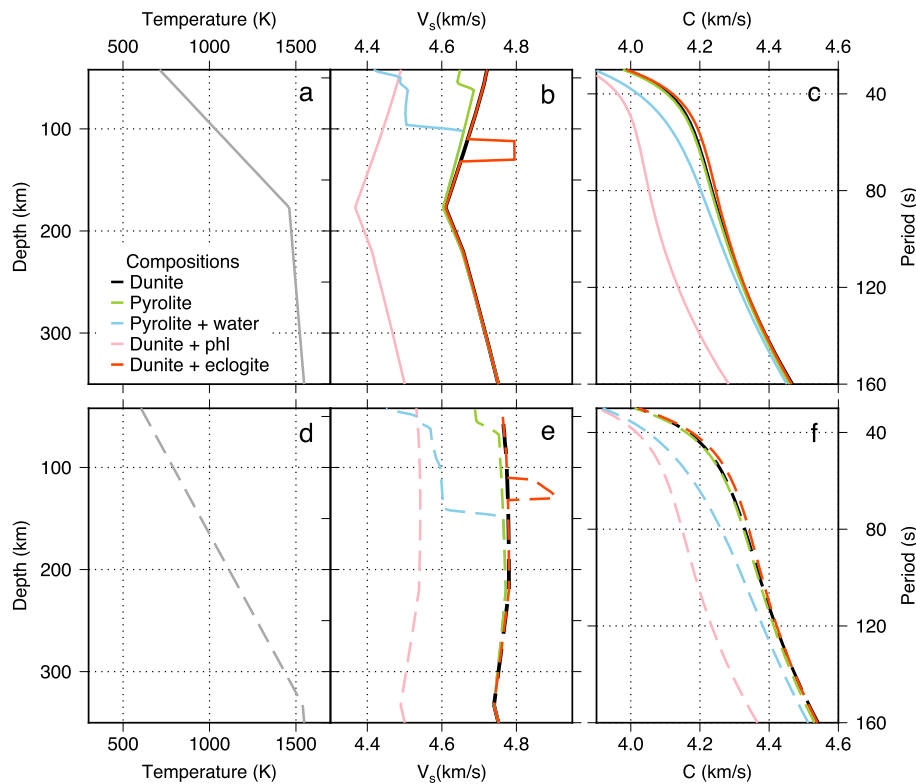


Fig. 4. (a,d) Two examples of cratonic geotherms for a sublithospheric potential temperature of 1100°C . Solid line for a surface heat flow of 44.0 mW m^{-2} , and dashed line for 37.0 mW m^{-2} . (b,e) Synthetic S wave velocity profiles and their (c,f) dispersion curves for a range of compositions. Note that refractory dunite (black), and fertile pyrolite (green) differ only slightly. For significantly lower or higher velocities we need a metasomatised composition (blue and pink) or the addition of a layer of eclogite (orange), respectively.

standard deviation of the data and as a function of frequency. The same uncertainties were assigned to all the groups.

2.2. Grid-search for thermo-chemical models

The dispersion structures of the groups described above were modelled by performing a grid search for forward-calculated thermo-chemical models that match the dispersion curves within their uncertainties, following the methods of Eeken et al. (2018), Eeken et al. (2020). The grid search can be divided into 3 basic steps: (1) We define a solution space of thermal and compositional mantle lithosphere/asthenosphere structures to search, (2) Each thermo-chemical structure is converted into seismic velocities as described in Eeken et al. (2018), using a thermodynamic approach (PerPleX, Connolly, 2005) that computes phase composition as a function of pressure and temperature (using the database from Holland and Powell, 1998) and then computes elastic parameters, density (using the database from Abers and Hacker, 2016) and anelasticity (following Faul and Jackson, 2005) for all depths below the crust. Crustal structure (with a range of uncertainties) is subsequently added based on previous studies. (3) For the given synthetic seismic structure, the code MINEOS (Masters et al., 2011) is used to calculate Rayleigh-wave fundamental mode dispersion curves. Nested loops in our code search through all different profiles and identify the ones that fit the observed average Rayleigh-wave dispersion curves within their uncertainties at all periods. Below we briefly summarise the thermo-compositional structures searched. More details can be found in the supplementary material (Section S2) and Eeken et al. (2018, 2020).

The thermal solution space captures a full range of plausible 1-D steady-state continental geotherms (see also Supplementary Section S2.1), spanning thermal lithospheric thicknesses (defined as the depth where the conductive geotherm and mantle adia-

bat intersect) from 120 to 350 km depth (Fig. 4), and a range of shapes, obtained by varying Moho heat flow and heat production in the mantle lithosphere. For the convecting mantle, we test adiabats with three different potential temperatures (1100° , 1200° , 1300°C).

For compositional structure (see also Supplementary Section S2.2), we test two end-member background compositions: a refractory dunite or a fertile pyrolite. The phase velocities for the refractory and fertile compositions are only subtly different (under 0.2%, Fig. 4) and therefore cannot explain the wide range of variation in phase velocities between the clusters (Fig. 3). Therefore, we additionally evaluate structures with layers of relatively seismically fast or slow mineralogies commonly found in xenoliths (Fig. 4). In defining these structures, we have borne in mind the limits in vertical resolution of the dispersion data, which is on the order of a few tens of km at 40 s, and 100–200 km at 160 s (see Eeken et al., 2020, for some examples of trade-offs between layer thicknesses, amplitudes, and depths).

Eclogite is the most common seismically fast mineralogy found in xenoliths (e.g. Pearson et al., 2003). Therefore, in cases where dispersion curves appear to require higher velocities in the mid-lithosphere, we test structures with an added layer of basaltic composition, which is substantially faster once the eclogite stability field has been entered (below about 70 km depth). Although differences in eclogitic velocities are larger than those in peridotitic velocities (Garber et al., 2018), all are substantially faster than any peridotitic composition (Fig. 4), and the choice of eclogite composition only changes best fitting layer thicknesses by a few km (Supplementary Fig. S4).

Metasomatic compositions are the most plausible seismically slow compositions expected under cratons (Bruneton et al., 2004; Eeken et al., 2018). As the seismic data only constrain velocity-depth distributions, we test for two common types of metaso-

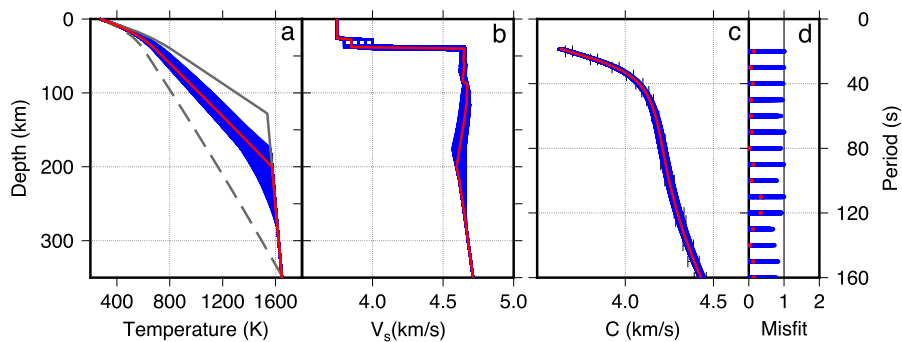


Fig. 5. All 435 acceptable solutions (out of 6030 searched) for Grenville group 4G (blue), for dunite with 0.5 wt% water and 1200°C mantle potential temperature. The minimum average misfit model is shown in red. The different panels are: (a) the geotherms accepted in the grid search are shown in blue, while the coldest and hottest geotherms tested are indicated by grey lines, (b) corresponding shear-wave velocity profiles, (c) corresponding Rayleigh-wave phase-velocity dispersion curves, and (d) misfit for each model.

matism that lead to a different depth distribution. Adding water as a metasomatic agent to our background compositions, amphibole, antigorite, and chlorite stabilise at depths above 100–150 km (Fig. 4(b)). However, because of their depth limitation, there is no significant effect for the longer periods. When some K_2O is added besides water, phlogopite mica is formed, which is stable throughout the lithosphere (Fig. 4(c)). We test compositions with a range of added water, as well as ones where water and K_2O are added in the proportions required to form different amounts of phlogopite. For the latter case, we assume that the amount of phlogopite decreases linearly with depth, as such a decrease was found to be required by the seismic data (Eeken et al., 2018). Other types of alteration (e.g. carbonates, high-P amphiboles) may well also contribute, but would require the addition of other components (e.g. CaO , CO_2) and are not seismically distinguishable from the compositions we test.

For the crust, regional seismic structures are assigned based on the literature cited in Section 1.2. For each crustal layer, we assign a fixed density, V_P , and V_S . To account for the uncertainties in crustal structure, we allow a range for lower crustal V_S and Moho depth (see Supplementary Table S3). Below the Moho, down to 400 km depth, the modelled thermo-chemical structure is converted to seismic velocities and densities as described above.

We also assumed a depth gradient in radial anisotropy, from 4% at 40 km depth to 0% at 220 km. This is within the range of radial anisotropy other studies have found within cratonic lithosphere (e.g., Dziewonski and Anderson, 1981; Yuan and Levin, 2014). There is some trade-off between assumed radial anisotropy and the compositional structures inferred. As shown by Eeken et al. (2018), solutions with strong radial anisotropy (up to 5% below the Moho) require less metasomatic alteration of the shallow lithosphere (up to 0.5 wt% less water, for cases with added water only, and up to 50% less phlogopite, for cases with added water and K_2O , compared to cases with zero radial anisotropy). Anisotropy does not trade-off with the thermal structure.

As an example of the results from the grid search process, we present a single set of solutions for group 4G for a refractory composition with 0.5 wt% water and a sublithospheric potential temperature of 1200°C (Fig. 5, for other regions see Figs. S5–S7). For the accepted solutions, the base of the thermal lithosphere, i.e. depth at which the geotherm intersects the mantle adiabat, ranges from 176 to 284 km (Fig. 5(a)). The corresponding velocity profiles (Fig. 5(b)) illustrate how the refractory composition plus water leads to a relatively low velocity directly below the Moho, which is required to match the dispersion curves (Fig. 5(c)).

3. Results

We summarise the main results below in figures that show the number of solutions for different choices of thermal and compositional structures. The relative numbers provide an overview of the most likely type of solutions and which regions are easier to fit (absolute numbers depend on the chosen size of the solution space and how finely it is sampled, Supplementary Section S2). Based on the compositional models with the highest number of solutions for each group, it is possible to divide the area of study into 4 major classes: (1) models where little to no metasomatic alteration is required to fit the dispersion curves, (2) models where significant alteration of the shallow mantle lithosphere is required, (3) models where more pervasive (stronger and/or deeper) metasomatism is required, and (4) models where high-velocity material at mid lithospheric depth is required. The solutions for the regions are discussed according to these classes below.

3.1. Unmodified lithosphere

Groups 1S and 3S, in the core of the western and eastern Superior, respectively, can be fit with lithospheric geotherms with dry or almost dry compositions, with water contents of 0 to 0.5 wt% (Fig. 6, for a complete overview of the acceptable solutions for all groups see Figs. S8–S17). If the lithosphere is assumed to have a refractory composition, then higher water contents are required to obtain low enough velocities directly below the Moho. The Western Superior has more solutions for a very cool sublithospheric temperature and requires low Moho heat flow, ($q_m = 10\text{--}14 \text{ mW m}^{-2}$). In contrast, the Eastern Superior solutions show a preference for warmer temperatures and higher q_m ($15\text{--}19 \text{ mW m}^{-2}$).

3.2. Upper lithosphere metasomatism

To match the relatively low velocities at shorter periods for groups 4P and 4G, metasomatic alteration of the shallow mantle lithosphere is required (Fig. 6). For these groups, the trade-off between the background composition and content of water becomes even more visible. Whatever background is chosen, an overall trend of increasing the amount of metasomatism from groups 1S and 3S to groups 4P and 4G is present. Additionally, both 4P and 4G have a preference for warmer asthenospheric temperatures, as well as higher Moho heat flow ($q_m = 14\text{--}21 \text{ mW m}^{-2}$).

As found previously (Boyce et al., 2016; Eeken et al., 2020), we also see a clear distinction between the eastern Superior (3S) and the Grenville (4G), where our data indicate that relatively low velocities are required in the shallow lithosphere of the eastern Canadian Grenville. Such findings corroborate the interpretation of

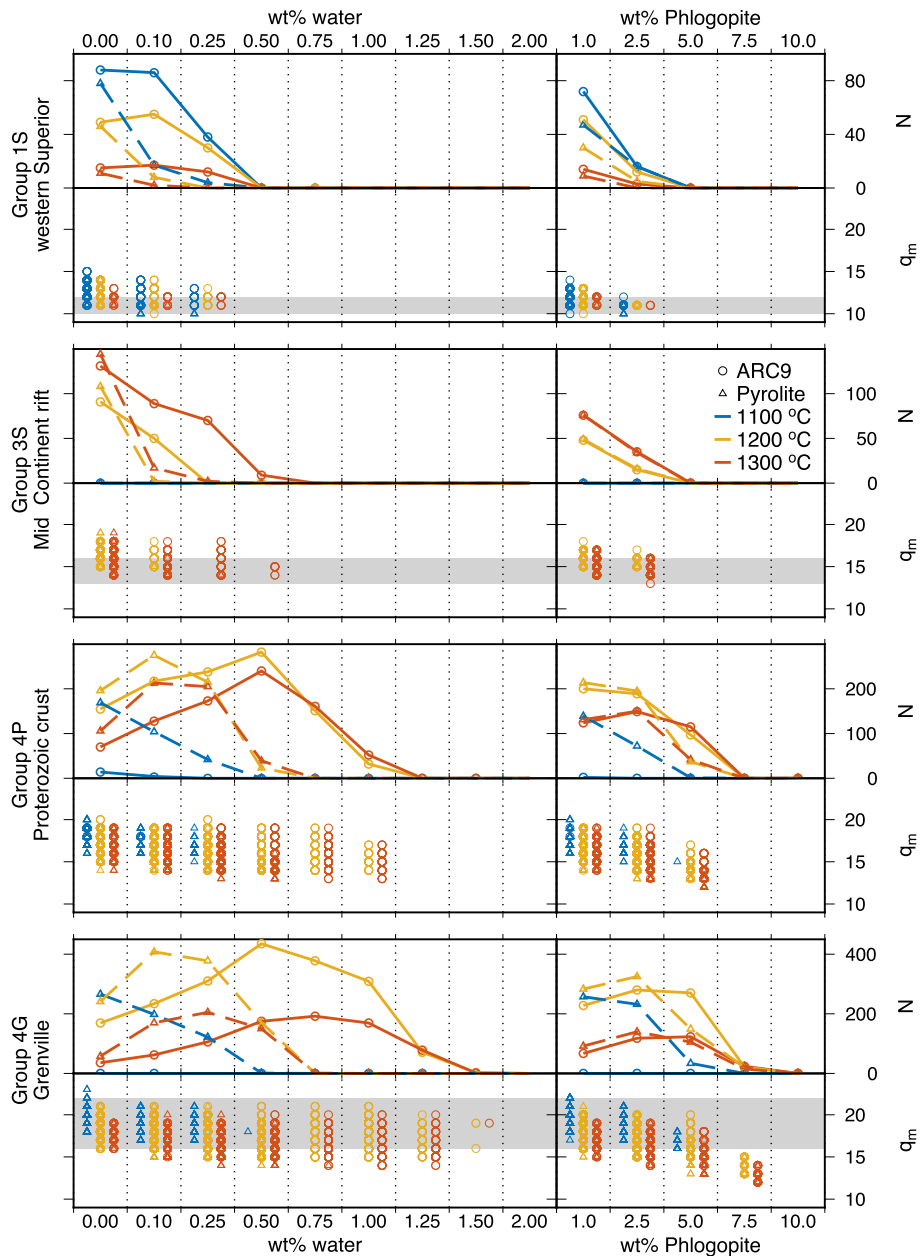


Fig. 6. Summary of the results for groups 1S (eastern Superior), 3S (western Superior), 4P (Proterozoic crust south of Mid-Centirent Rift), and 4G (Grenville) in terms of number of solutions (N) and Moho heat flow (q_m) for different sublithospheric potential temperatures (represented by different colours) as function of the amount of water (in wt%) or as a function of the amount of phlogopite, added to a dunite or pyrolite background (represented by different line styles/symbols). Our solutions are generally consistent with the range of Moho heat flow for the region inferred from heat flow and heat production by Shapiro et al. (2004) and Levy et al. (2010) (shaded grey). The amount of water required increases from groups 1S and 3S to groups 4P and 4G. Note that there is a trade off between the background composition and water content.

modification by metasomatism of the Laurentian margin due to subduction beneath the continent in the Grenville region (4G) and, by correlation, the Proterozoic terranes in region 4P.

3.3. More pervasive metasomatism

The southern Superior (4S), the Mid-Centirent Rift System (5M), the proposed continuation of the St. Lawrence rift system (5G), and the Rome Trough rift (6G) groups are in regions affected by rifting. These all require stronger and possibly deeper metasomatism (Fig. 7) than the regions in Fig. 6.

Group 4S requires significant water content in the shallow lithosphere as well as relatively cool sublithospheric temperatures. Most of our solutions have relatively high q_m , except for models with significant amounts of phlogopite (>5 wt%). Previous studies,

using heat flow and heat production data, have inferred for this region a relatively low Moho heat flow, similar to that of region 3S (13–14 mW m^{-2} , Levy et al. (2010); Perry et al. (2006b)). Such low q_m would be only consistent with modification throughout the lithosphere and a relatively thick thermal lithosphere.

Results for group 5M require little water or phlogopite, similar to regions 3S and 1S. The main difference between 5M and these regions is the significantly thicker crust which leads to quite low phase velocities at periods shorter than 50 s. Surface heat flow in the western part of Lake Superior is low (<30 mW m^{-2} , Perry et al. (2006b)), and the estimated Moho heat flow is lower than 12 mW m^{-2} (Shapiro et al., 2004). Similar to group 4S, for a low q_m , the preferred compositional solutions are those with some alteration throughout the lithosphere.

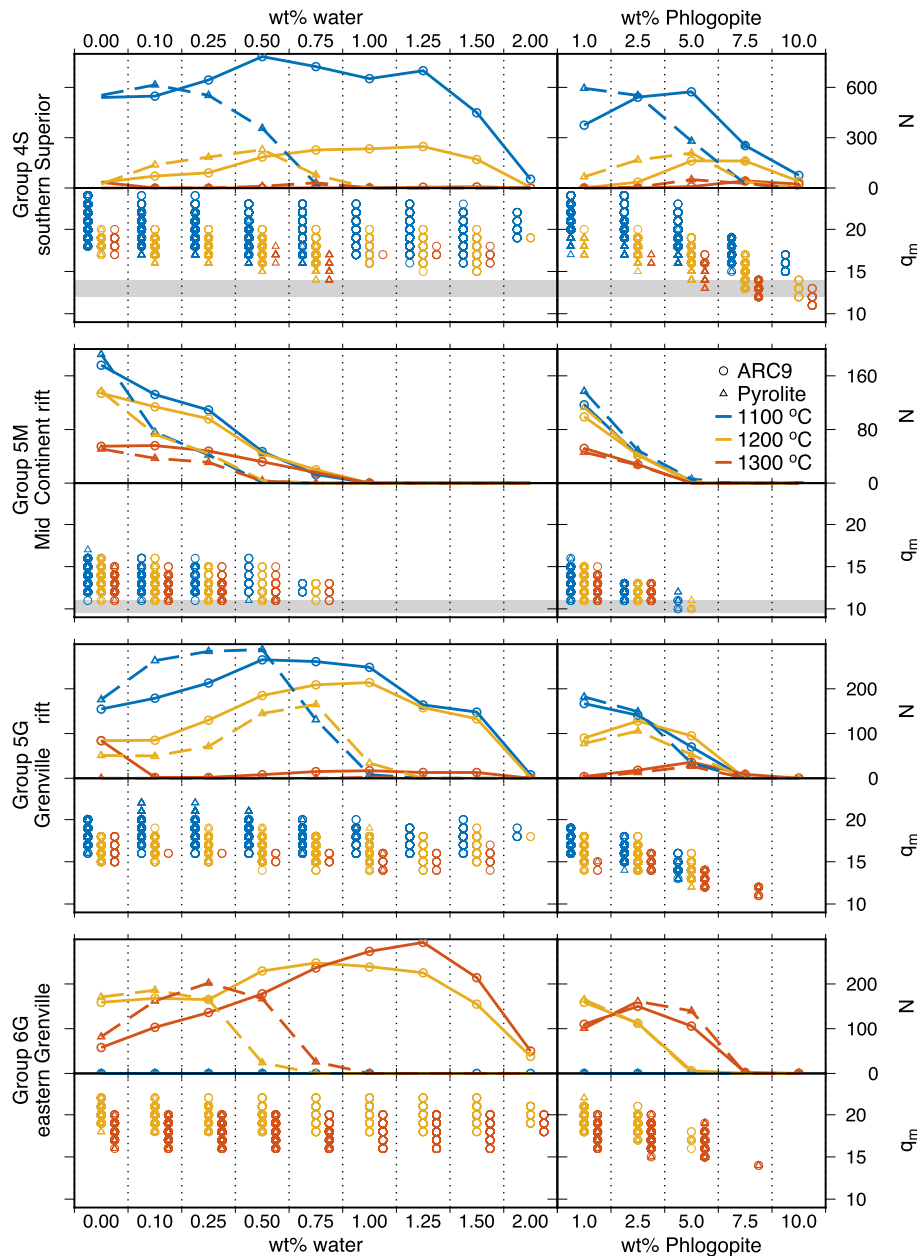


Fig. 7. Summary of the results for groups 4S (southern Superior), 5M (Mid-Continent rift), 6G (eastern Grenville) and 5G (Grenville - St. Lawrence Rift) in terms of number of solutions (N) and Moho heat flow (q_m) for different sublithospheric potential temperatures (represented by different colours) as a function of the amount of water (in wt%) or as a function of the amount of phlogopite, added to a dunite or pyrolite background (represented by different line styles/symbols). The range of Moho heat flow inferred by Shapiro et al. (2004) and Levy et al. (2010) for regions 4S and 5M (shaded grey) is most consistent with solutions with alteration throughout the lithosphere.

Compared to 4G, group 5G has a thicker crust which leads to quite low phase velocities at short periods, but additionally, solutions favour stronger mantle lithosphere alteration than group 4G, as well as cooler sub-lithospheric temperatures. There is no well-constrained heat-flow based estimate of q_m for this region. Surface heat flow values are similar to or lower than those of the Grenville in region 4G (35–40 mW m^{-2} , Levy et al. (2010); Goes et al. (2020)). If heat production is similar to that of region 4G and the additional crustal thickness is the result of underplating of relatively low heat-production mafic material, then Moho heat flow is likely to be similar to or lower than region 4G. For q_m between 14 and 19 mW m^{-2} , either substantial hydrous alteration confined to the shallower lithosphere or phlogopite alteration throughout provide acceptable fits.

Results for Group 6G show a preference for stronger metasomatism and hotter sublithospheric temperature than for the other

regions in the Grenville. Surface heat flow is relatively high (increasing from west to east with an average of 52 mW m^{-2} , Frone et al. (2015)), as are estimates of Moho temperature from P_n (Goes et al., 2020) suggesting a relatively high q_m of around 18–22 mW m^{-2} , most consistent with solutions of substantial hydrous alteration confined to the shallower lithosphere.

Groups 5M and 4S are in regions affected by the Mid-Continent Rift System. Such activity may have brought fluids to the system from below, which would explain the metasomatic alteration of the whole continental lithosphere. Interestingly, while the crustal expression of this event mainly lies in 5M, the mantle signature appears stronger below 4S. Our results also support a distinction between the north and south Grenville as proposed by Boyce et al. (2019), and we interpret the difference in velocity as a possible result of the joint alteration effects of magmatism associated with collision and rifting.

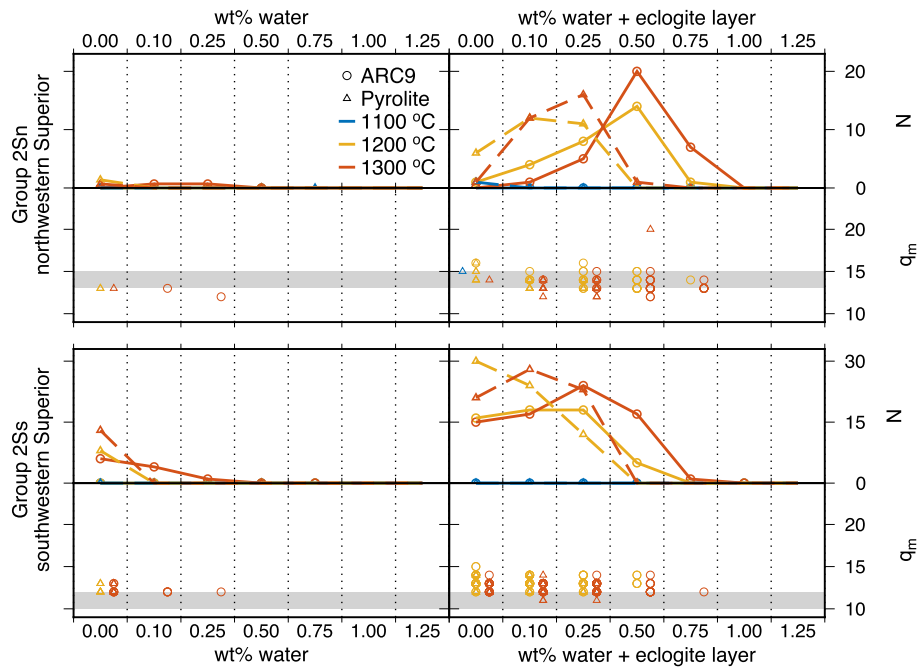


Fig. 8. Summary of the results for groups 2Sn (northwestern Superior) and 2Ss (southwestern Superior) in terms of number of solutions (N) and Moho heat flow (q_m) for different sublithospheric potential temperatures (represented by different colours) as a function of the amount of water (in wt%) or the amount of water plus a layer of eclogite, added to a dunite or pyrolite background (represented by different line styles/symbols). These groups require a layer of eclogite between 110 and 130 km depth with water added on top. The range of Moho heat flow inferred by Shapiro et al. (2004) and Levy et al. (2010) (shaded grey) is similar to the low q_m from our solutions.

3.4. Lithosphere with a high-velocity layer

A few kinds of structures could fit the dispersion curves for Groups 2Sn and 2Ss, in the north and south of the western Superior, respectively. Those groups have relatively constant phase velocities with period, which require a structure where a high-velocity layer overlays low-velocity material. We can achieve this either by adding a low-velocity layer at greater depths in/below quite cold lithosphere or high-velocity material at shallower depths in somewhat warmer lithosphere. We also tested adding a layer of low-velocity material at the top of the asthenosphere. While this can match phase velocities, the temperatures in such a layer would be too low for partial melting and the velocity drop would require high degrees of alteration (e.g. >5 wt% phlogopite), raising questions about the layer's origin and stability. As another option, we could strongly increase the radial anisotropy at the base of the lithosphere, which trades off with temperature and metasomatic mineral contents as will be discussed below. Alternatively, we can add a layer of eclogite in the mid lithosphere. We have tested for various depth distributions, and find most solutions for a layer from 110 to 130 km depth with various amounts of added water on top (Fig. 8). A thickness of 20 km is compatible that expected for oceanic crust formed at Archean mantle temperatures (Weller et al., 2019).

The presence of a mid-lithospheric eclogitic layer is consistent with the seismic profile from the Lithoprobe project in region 2Ss. The project imaged a high-velocity layer dipping from south to north that was interpreted as remnant oceanic lithosphere accreted during the assembly of the Superior Province (Musacchio et al., 2004). Similarly, the 2Sn group is close to the Trans-Hudson Orogen, where Miller and Eaton (2010) found dipping high-velocity layers associated with ancient subduction and accretion to form Laurentia's core.

Garber et al. (2018) found that globally averaged cratonic seismic structures (in particular from waveform-derived model SE-MUCB_WM1 (French and Romanowicz, 2014)) often contain high velocities between 120 and 150 km depth. They suggest that these

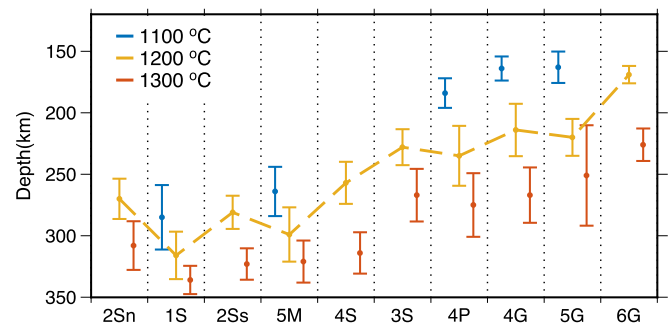


Fig. 9. Summary of the standard deviation of lithospheric thickness for each of the three tested sublithospheric potential temperatures (blue for 1100 °C, yellow for 1200 °C, and orange for 1300 °C). We used for this figure the chemical solutions that best represent each group: for 2Sn (northwestern Superior) and 2Ss (southwestern Superior) - solutions with added water in the range 0.0-2.0 wt% underlain by a layer of eclogite; for 1S (western Superior), 3S (eastern Superior), 4P (Proterozoic south of Mid-Centinet Rift), 4G (Grenville), 5G (Grenville-St. Lawrence Rift), and 6G (eastern Grenville) - solutions with added water in the range 0.0-2.0 wt%; for 4S (southern Superior), 5M (Mid-Centinet Rift) - solutions with 1-10% phlogopite. Note that there is a trade off between sublithospheric temperature and thermal lithospheric thickness. Since a dramatic change of sublithospheric temperature is unlikely between the groups, we suggest that there is a systematic variation in lithospheric thickness across the study region (dashed yellow line).

velocities can be explained by an additional 20 vol% eclogite and 2 vol% diamond around these depths. Given the non-uniqueness of tomographically-derived velocity profiles, it would be of interest to test whether our regionally variable structures, including layers of eclogite, can also match the waveform data.

3.5. Thermal lithospheric thickness variation

Most regions have solutions for all three sublithospheric temperatures tested (Fig. 9). Within the acceptable solutions, it is possible that lithospheric thickness is large (around 270 km), and does not vary much below most of the region. However, that would require variations of 100-200 °C in asthenospheric temperatures

below the Superior. It would be difficult to maintain such different temperatures between close areas within the convecting mantle.

There is a trade-off between sublithospheric temperature and the thermal lithospheric thickness: for a cold asthenosphere, a thinner lithosphere is better able to match the dispersion data than it is for a warmer asthenosphere. Therefore, we suggest that what we see is likely a systematic variation in lithospheric thickness across the study region. Taking 1200 °C as the background asthenospheric potential temperature (as we have solutions for all regions for this temperature), the results indicate that the lithosphere is systematically thicker below the Western Superior (groups 1S, 2S, and 5M, 250–340 km) than below the southeastern Superior and neighbouring Proterozoic regions (groups 3S, 4P, 4G, 190–260 km) and is thinnest below the southeasternmost Grenville (group 6G, 160–180 km). Within the western Superior, the lithosphere below 2Sn and 2Ss is around 30 km thinner than the core region 1S. Interestingly, the lithospheric thickness of the zones characterised by surface rifting (5M, 5G, and 6G) is not distinct from that of neighbouring regions, indicating that either lithospheric thinning did not occur directly below the surface expression, but instead may have occurred below, for example, region 4S (240–270 km thick), or that the thinned lithosphere has since thermally equilibrated to a thickness similar to that of the surrounding lithosphere. When we combine these results with those from Eeken et al. (2020), the Superior Province includes two thick highly depleted cores, in the northeast and west, while the intervening region 3S is less refractory or slightly more altered, and thinner.

4. Discussion

4.1. Uncertainties

The method involves a range of uncertainties associated with the data, our choice of parameters for the grid search inversion, and the trade-offs between them. Here we will discuss some of the main uncertainties related to the extracted dispersion curves, the thermodynamic methods, the attenuation model, and lithospheric radial anisotropy.

The dispersion curves are the product of an inversion that involves smoothing and damping (Foster et al., 2020). To minimise edge effects, regularisation effects, and variations in model resolution, we removed from our analysis the points on the edge of the original study area, where resolution decreases. Additionally, we are only analysing regions that can be resolved based on the checkerboard tests from Foster et al. (2020). Because of the smoothing and resolution, our results can only represent large-scale lithospheric structure (e.g. over 300 km lateral extent). For example, we do not distinguish anomalies of the scale of the Great Meteor hotspot.

There are also uncertainties associated with the thermodynamic methods (including the choice of equation of state and its parameters, solid-solution models, and averaging of end-member compositions) and databases (e.g. Eeken et al., 2018; Garber et al., 2018). However, the seismic data require velocity variations that significantly exceed the uncertainties in the synthetic velocities for any single composition considered here. Moreover, the seismic data do not uniquely constrain the variation of velocity with depth but do require several distinct classes of structure containing high and/or low-velocity layers. The high velocities are too high for any composition on the fertile to refractory peridotite array, but can be matched with layers of an eclogitic composition of a reasonable thickness. A different choice of eclogite does not change the required thicknesses by more than a few km. Similarly, where low-velocity layers are required, various combinations

of metasomatic minerals will be able to satisfy the seismic constraints, not only the limited set of hydrous compositions considered here, but also combinations including carbonate minerals and/or high-temperature amphiboles. The metasomatic mineralogies we considered are mineralogies commonly found in xenoliths and form readily when some water is added to a potentially quite refractory peridotite. Our calculations provide constraints on the relative intensity of metasomatic alteration required in different regions, as well as some constraints on the depth distribution.

Other uncertainties are related to the chosen attenuation and radial anisotropy models. The choice of attenuation model affects the forward modelled velocity-depth gradients. We use the anelasticity model QF (Faul and Jackson, 2005), which has a relatively strong temperature dependence. Because anelastic effects are only significant at the base of the lithosphere and the mantle below (Goes et al., 2012), the choice of anelasticity may shift estimates of thermal thickness (by a few tens of km), but the style of our solutions, the relative variations in thickness and different classes we infer are not affected.

Radial anisotropy estimates in models for cratonic lithosphere usually range between 0 and 5% anisotropy. They are often similar to PREM, where the radial anisotropy is highest directly below the Moho and decreases with depth (e.g., Freybourger et al., 2001; Dziewonski and Anderson, 1981), but other more complex structures have also been imaged (Yuan and Romanowicz, 2010). As mentioned, we use a simple model of anisotropy (similar to PREM) for all regions. Therefore, we do not account for variations in anisotropy vertically (between layers) or laterally (between the groups). If we were to include stronger or more variable radial anisotropy, the consequence would be higher isotropic velocities, thus requiring lower amounts of metasomatism, although the thermal characteristics would remain similar (Eeken et al., 2018). Optimally, in the future, a combined Rayleigh and Love wave analysis would be used to provide direct constraints on radial anisotropy.

4.2. Lithospheric thickness variations

There can be different causes for lithospheric thickness variations. We have defined thermal thickness as the intersection between the conductive geotherm and mantle adiabat. This parameterisation is an approximation of the expected thermal structure which would include a transitional layer between the conductive lid and the convecting mantle. For temperatures above about 1100 °C the lithosphere may reach an actual conductive steady state. However, seismic data are most sensitive to the depth of the velocity minimum, which forward models predict lies close to where the extrapolated conductive geotherm would intersect the adiabat.

Numerical models (e.g., Cooper et al., 2004) show that temporal variations in thermal thickness as we define it here occur due to instability of the transitional layer at the base of the lithosphere. Such instabilities may occur on time scales of tens of Myr, and over thicknesses of a few tens of km for the high viscosities expected for thick lithosphere. Additionally, variations in composition may lead to stabilisation of the lithosphere to different depths (Cooper et al., 2004; Wang et al., 2014). The difference in thickness between regions 1S and 3S could reflect the latter process if amalgamation of the craton has resulted in juxtaposition of lithospheric blocks that are distinct in their compositionally controlled stability. The relatively thick lithosphere below the Mid-Continent Rift system might have formed when mantle from which large amounts of melt were extracted cooled to form relatively low density and high viscosity lithosphere, while alteration of the lithosphere below 4S may have led to a smaller long-term thickness.

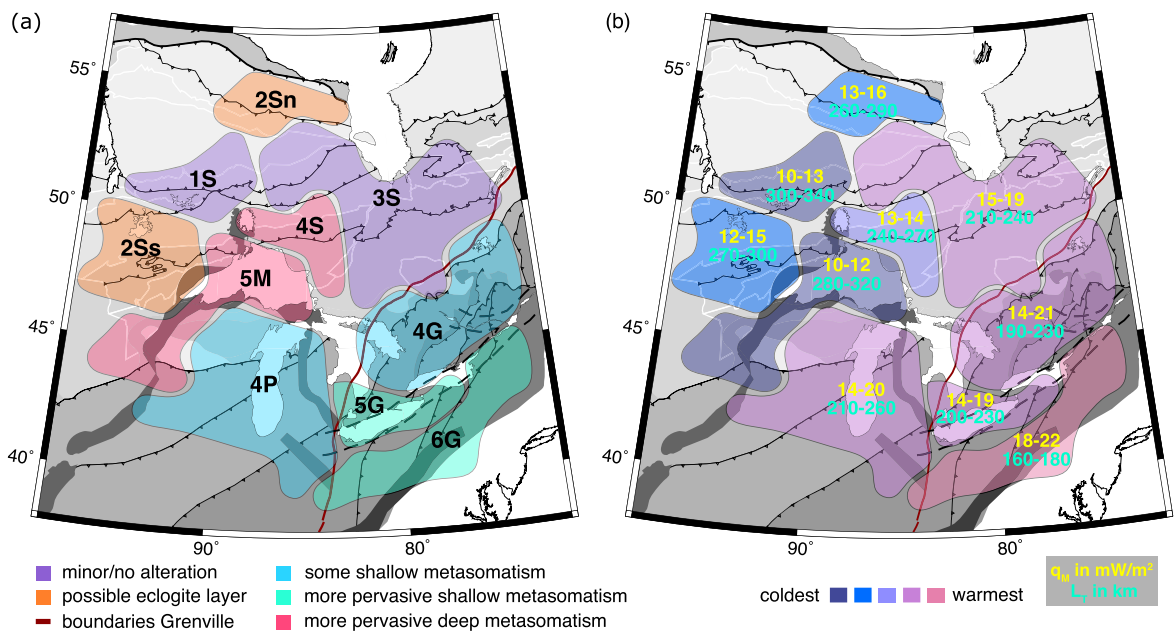


Fig. 10. Summary map of the compositional (a) and thermal (b) variation across the study region inferred from our results. Groups in the Superior Province 2Sn and 2Ss are regions that require an eclogite layer with various amounts of water added. The western (1S) and eastern (3S) cores of the Superior Province are regions that are best fit by a dry or almost dry composition. The regions of Proterozoic arc accretion, 4P and 4G, require some metasomatic alteration in the shallow lithosphere. Regions affected by the Mid-Continent Rift (4S and 5M) require more pervasive metasomatic alteration that extends into the deeper lithosphere, while the rift regions in the Grenville (5G and 6G) require more pervasive metasomatism either concentrated mainly shallowly or extending deeper. In thermal structure, there is an overall northwest to southeast warming/thinning of the lithosphere below the study region.

4.3. Structure and tectonics

Emerging from this work and a few previous studies is the conclusion that lithospheric mantle below continental shields holds more of a record of its previous tectonic history than previously thought. Beside a dry lithosphere in the core cratonic regions, we observe three to four other classes of lithospheric structure: upper lithosphere metasomatism, upper lithosphere metasomatism above an eclogitic layer, more pervasive metasomatism, potentially extending to larger depths (Fig. 10).

Upper-lithosphere metasomatism is required beneath regions 4P and 4G. We interpret the upper lithosphere modification by metasomatism on the Laurentian margin due to subduction beneath the continent. A few other studies have also noted significant slow velocity anomalies in the shallow lithosphere below regions known to have been affected by significant arc-related magmatism in the Proterozoic (e.g., Boyce et al., 2019; Liddell et al., 2018; Legendre et al., 2012; Eeken et al., 2020).

The signature of Archean and Paleoproterozoic subduction appears to be distinct from that below younger Proterozoic regions. Although slow velocities in the shallow mantle lithosphere improve the dispersion curve fit, regions 2Sn and 2Ss require a relatively high-velocity mid lithosphere. This velocity anomaly can be matched by a mid-lithospheric layer of eclogite (10–20 km thick), which might well correspond to relict subducted oceanic crust. Eeken et al. (2020) also required a similar structure to match dispersion data below the extension of the Trans Hudson Orogen below James Bay (just north of region 3S). The presence of such layers is consistent with refraction profiles and S receiver functions that image dipping high-velocity layers below these or nearby regions, as mentioned in Section 3.4. Similar structures of dipping high-velocity material have also been imaged in several other cratons, including the Slave (Bostock, 1998) and Wyoming Cratons (Hopper and Fischer, 2015). There too, these features have been interpreted as related to shallow subduction in Archean/Paleoproterozoic time. Archean/Paleoproterozoic subduction may well

have been different from more recent subduction styles, as thicker oceanic crust and more buoyant and stronger mantle lithosphere might have favoured shallow subduction (e.g., Abbott, 1991; van Hunen and Moyen, 2012).

The final one to two classes, of more pervasive metasomatism, comprise regions affected by rifting. Regions 5M and 4S were affected by the formation of the Mid-continent Rift system. Given that surface heat flow plus constraints on heat production indicate low Moho heat flow (Shapiro et al., 2004; Levy et al., 2010), those regions require metasomatic alteration throughout the lithosphere, which we interpret as an expression of modification after assembly. Plume activity and rifting could lead to the infiltration of magmatic fluids into the cratonic keel, causing metasomatism (Lee and Rudnick, 1999). Regions 5G and 6G in the eastern Grenville were also affected by rift systems, in this case, during the break up of the Rodinia supercontinent. The near-surface expressions include a thick crust and basin formation. Those regions at least require more pervasive shallow modification than region 4G, potentially extending to larger depth. This extensive alteration could be the result of the superposition of modification during subduction event and further alteration associated with later rifting. Boyce et al. (2019) inferred a similar difference in metasomatic alteration from less extensive in the northern Grenville (our region 4G and northwards) to more pervasive modification in the southern Grenville (our regions 5G, 6G and southwards).

These classes of structure may thus reflect processes of formation and modification of the lithosphere. These findings agree with geochemical and petrological analyses on xenoliths which document temporal and spatial variations in composition due to formation and modification of the lithospheric mantle by different styles of metasomatism (Scully et al., 2004; Hunt et al., 2012; Wyman et al., 2014). Variation in composition like what we find here may also help to explain observations of seismic mid-lithospheric discontinuities of both negative and positive polarity, which could be due to layered metasomatic alteration and eclogite layers.

5. Conclusions

Variations in Rayleigh-wave dispersion curves across the eastern Canada/Great Lakes region can be modelled with four to five distinct types of thermo-chemical mantle lithosphere once we account for regional crustal structure. The eastern and western cores of the Archean Superior Province can be matched with a dry/almost dry composition. Regions of Proterozoic arc accretion in the eastern margin of Laurentia require metasomatic alteration of the shallow mantle lithosphere, while regions of collision in the Trans-Hudson Orogen and the southern Superior are characterised by a high-velocity mid-lithospheric layer, which we interpret as remnant subducted thick oceanic crust, consistent with interpretations of nearby refraction profiles. This is further evidence of distinct modes of subduction and accretion in the later Proterozoic and Archean. Regions affected by rifting require more pervasive metasomatism. For the Mid-Century Rift as well as the region immediately north of it (including the Nipigon arm of the rift) heat flow constraints favour solutions where this alteration extends into the deep lithosphere, likely a signature of modification by magmatic fluids from below. The rift structures in the Grenville require more pervasive metasomatic alteration of the shallow lithosphere which may or may not extend throughout the lithosphere. We interpret this as a result of the joint effects of a Proterozoic collision and later rifting.

In addition to these systematic compositional variations that reflect tectonic history, the thermal lithospheric thickness and Moho heat flow varies considerably across the region. The western Superior core is thickest and coldest, reaching 320 km depth, while the eastern Grenville is the warmest and only around 170 km thick. These results provide a context for reevaluating other studies of the structure of continental shields, e.g. those of mid-lithospheric discontinuities, as they may reflect similar tectonically controlled structures.

Declaration of competing interest

The authors declare that they have no known competing financial interests or personal relationships that could have appeared to influence the work reported in this paper.

Acknowledgements

We thank Barbara Romanowicz for discussions, Suzan Van der Lee for thoughtful comments that helped us to improve the manuscript, and Joshua Garber and an anonymous reviewer for their constructive reviews. Isabella L. Altoe is supported by a scholarship from the CAPES Foundation, agency under the Ministry of Education, Brazil (DOC_PLENO - 88881.128245/2016-01). Fiona Darbyshire and Anna Foster are supported by the Natural Sciences and Engineering Research Council of Canada (NSERC) through the Discovery Grants and Canada Research Chair programmes (341802-2013-RGPN).

Appendix A. Supplementary material

Supplementary material related to this article can be found online at <https://doi.org/10.1016/j.epsl.2020.116465>.

References

- Abbott, D., 1991. The case for accretion of the tectosphere by buoyant subduction. *Geophys. Res. Lett.* 18, 585–588. <https://doi.org/10.1029/91GL00813>.
- Abers, G.A., Hacker, B.R., 2016. A Matlab toolbox and Excel workbook for calculating the densities, seismic wave speeds, and major element composition of minerals and rocks at pressure and temperature. *Geochem. Geophys. Geosyst.* 17, 616–624. <https://doi.org/10.1002/2015GC006171>.
- Abt, D.L., Fischer, K.M., French, S.W., Ford, H.A., Yuan, H., Romanowicz, B., 2010. North American lithospheric discontinuity structure imaged by Ps and Sp receiver functions. *J. Geophys. Res., Solid Earth* 115, B09301. <https://doi.org/10.1029/2009JB006914>.
- Bollmann, T.A., Lee, S., Frederiksen, A.W., Wolin, E., Revenaugh, J., Wiens, D.A., Darbyshire, F.A., Stein, S., Wysession, M.E., Jurdy, D., 2019. P wave teleseismic traveltimes tomography of the North American Midcontinent. *J. Geophys. Res., Solid Earth* 124, 1725–1742. <https://doi.org/10.1029/2018JB016627>.
- Bostock, M.G., 1998. Mantle stratigraphy and evolution of the Slave province. *J. Geophys. Res., Solid Earth* 103, 21183–21200. <https://doi.org/10.1029/98jb01069>.
- Boyce, A., Bastow, I.D., Darbyshire, F.A., Ellwood, A.G., Gilligan, A., Levin, V., Menke, W., 2016. Subduction beneath Laurentia modified the eastern North American cratonic edge: evidence from P wave and S wave tomography. *J. Geophys. Res., Solid Earth* 121, 5013–5030. <https://doi.org/10.1002/2016JB012838>.
- Boyce, A., Bastow, I.D., Golos, E.M., Rondenay, S., Burdick, S., Van der Hilst, R.D., 2019. Variable modification of continental lithosphere during the Proterozoic Grenville orogeny: evidence from teleseismic P-wave tomography. *Earth Planet. Sci. Lett.* 525, 115763. <https://doi.org/10.1016/j.epsl.2019.115763>.
- Boyce, J.L., Morris, W.A., 2002. Basement-controlled faulting of Paleozoic strata in southern Ontario, Canada: new evidence from geophysical lineament mapping. *Tectonophysics* 353, 151–171. [https://doi.org/10.1016/S0040-1951\(02\)00280-9](https://doi.org/10.1016/S0040-1951(02)00280-9).
- Bruneton, M., Pedersen, H.A., Vacher, P., Kukkonen, I.T., Arndt, N.T., Funke, S., Friederich, W., Farra, V., 2004. Layered lithospheric mantle in the central Baltic Shield from surface waves and xenolith analysis. *Earth Planet. Sci. Lett.* 226, 41–52. <https://doi.org/10.1016/j.epsl.2004.07.034>.
- Buchan, K.L., Ernst, R.E., 2004. *Essais de dykes de diabase et unités apparentées au Canada et dans les régions avoisinantes*. Technical Report. Geological Survey of Canada, "A" Series Map 2022A.
- Calvert, A.J., Sawyer, E.W., Davis, W.J., Ludden, J.N., 1995. Archean subduction inferred from seismic images of a mantle suture in the Superior Province. *Nature* 375, 670–674. <https://doi.org/10.1038/375670a0>.
- Cannon, W.F., Lee, M.W., Hinze, W.J., Schulz, K.J., Green, A.G., 1991. Deep crustal structure of the Precambrian basement beneath northern Lake Michigan, midcontinent North America. *Geology* 19, 207. [https://doi.org/10.1130/0091-7613\(1991\)019<0207:DCSOTP>2.3.CO;2](https://doi.org/10.1130/0091-7613(1991)019<0207:DCSOTP>2.3.CO;2).
- Chen, C.W., Li, A., 2012. Shear wave structure in the Grenville Province beneath the lower Great Lakes region from Rayleigh wave tomography. *J. Geophys. Res., Solid Earth* 117. <https://doi.org/10.1029/2011JB008536>.
- Clowes, R.M., 2010. Initiation, development, and benefits of Lithoprobe – shaping the direction of Earth science research in Canada and beyond. *Can. J. Earth Sci.* <https://doi.org/10.1139/E09-074>.
- Connolly, J., 2005. Computation of phase equilibria by linear programming: a tool for geodynamic modeling and its application to subduction zone decarbonation. *Earth Planet. Sci. Lett.* 236, 524–541. <https://doi.org/10.1016/j.epsl.2005.04.033>.
- Cooper, C., Lenardic, A., Moresi, L., 2004. The thermal structure of stable continental lithosphere within a dynamic mantle. *Earth Planet. Sci. Lett.* 222, 807–817. <https://doi.org/10.1016/j.epsl.2004.04.008>.
- Darbyshire, F.A., Eaton, D.W., Bastow, I.D., 2013. Seismic imaging of the lithosphere beneath Hudson Bay: episodic growth of the Laurentian mantle keel. *Earth Planet. Sci. Lett.* 373, 179–193. <https://doi.org/10.1016/j.epsl.2013.05.002>.
- Darbyshire, F.A., Eaton, D.W., Frederiksen, A.W., Ertolahti, L., 2007. New insights into the lithosphere beneath the Superior Province from Rayleigh wave dispersion and receiver function analysis. *Geophys. J. Int.* 169, 1043–1068. <https://doi.org/10.1111/j.1365-246X.2006.03259.x>.
- Dziewonski, A.M., Anderson, D.L., 1981. Preliminary reference Earth model. *Phys. Earth Planet. Inter.* 25, 297–356. [https://doi.org/10.1016/0031-9201\(81\)90046-7](https://doi.org/10.1016/0031-9201(81)90046-7).
- Eaton, D.W., Dineva, S., Mereu, R., 2006. Crustal thickness and VP/VS variations in the Grenville orogen (Ontario, Canada) from analysis of teleseismic receiver functions. *Tectonophysics* 420, 223–238. <https://doi.org/10.1016/j.tecto.2006.01.023>.
- Eeken, T., Goes, S., Pedersen, H.A., Arndt, N.T., Bouilhol, P., 2018. Seismic evidence for depth-dependent metasomatism in cratons. *Earth Planet. Sci. Lett.* 491, 148–159. <https://doi.org/10.1016/j.epsl.2018.03.018>.
- Eeken, T., Goes, S., Petrescu, L., Altoe, I., 2020. Lateral variations in thermochemical structure of the Eastern Canadian Shield. *J. Geophys. Res., Solid Earth.* <https://doi.org/10.1029/2019JB018734>.
- Ernst, R., Bleeker, W., 2010. Large igneous provinces (LIPs), giant dyke swarms, and mantle plumes: significance for breakup events within Canada and adjacent regions from 2.5 Ga to the present. *Can. J. Earth Sci.* 47, 695–739. <https://doi.org/10.1139/E10-025>.
- Faul, U.H., Jackson, I., 2005. The seismological signature of temperature and grain size variations in the upper mantle. *Earth Planet. Sci. Lett.* 234, 119–134. <https://doi.org/10.1016/j.epsl.2005.02.008>.
- Foster, A., Darbyshire, F., Schaeffer, A., 2020. Anisotropic structure of the central North American Craton surrounding the Mid-Century Rift: evidence from Rayleigh waves. *Precambrian Res.* <https://doi.org/10.1016/j.precamres.2020.105662>.
- Frederiksen, A.W., Bollmann, T., Darbyshire, F., Van Der Lee, S., 2013. Modification of continental lithosphere by tectonic processes: a tomographic image of central North America. *J. Geophys. Res., Solid Earth* 118, 1051–1066. <https://doi.org/10.1002/jgrb.50060>.

- Frederiksen, A.W., Miong, S.K., Darbyshire, F.A., Eaton, D.W., Rondenay, S., Sol, S., 2007. Lithospheric variations across the Superior Province, Ontario, Canada: evidence from tomography and shear wave splitting. *J. Geophys. Res.* 112, B07318. <https://doi.org/10.1029/2006JB004861>.
- French, S.W., Romanowicz, B.A., 2014. Whole-mantle radially anisotropic shear velocity structure from spectral-element waveform tomography. *Geophys. J. Int.* 199, 1303–1327. <https://doi.org/10.1093/gji/ggu334>.
- Freybourger, M., Gaherty, J.B., Jordan, T.H., 2001. Structure of the Kaapvaal Craton from surface waves. *Geophys. Res. Lett.* 28, 2489–2492. <https://doi.org/10.1029/2000GL012436>.
- Frone, Z., Blackwell, D., Richards, M., Hornbach, M., 2015. Heat flow and thermal modeling of the Appalachian basin, West Virginia. *Geosphere* 11, 1279–1290.
- Garber, J.M., Maurya, S., Hernandez, J.A., Duncan, M.S., Zeng, L., Zhang, H.L., Faul, U., McCammon, C., Montagner, J.P., Moresi, L., Romanowicz, B.A., Rudnick, R.L., Stixrude, L., 2018. Multidisciplinary constraints on the abundance of diamond and eclogite in the cratonic lithosphere. *Geochim. Geophys. Geosyst.* 19, 2062–2086. <https://doi.org/10.1029/2018GC007534>.
- Gilligan, A., Bastow, I.D., Darbyshire, F.A., 2016. Seismological structure of the 1.8 Ga Trans-Hudson Orogen of North America. *Geochim. Geophys. Geosyst.* 17, 2421–2433. <https://doi.org/10.1002/2016GC006419>.
- Goes, S., Armitage, J., Harmon, N., Smith, H., Huisman, R., 2012. Low seismic velocities below mid-ocean ridges: attenuation versus melt retention. *J. Geophys. Res.* B, Solid Earth Planets 117. <https://doi.org/10.1029/2012JB009637>.
- Goes, S., Hasterok, D., Schutt, D., Klöcking, M., 2020. Continental lithospheric temperatures: a review. *Phys. Earth Planet. Inter.* <https://doi.org/10.1016/j.pepi.2020.106509>, in press.
- Griffin, W.L., O'Reilly, S.Y., Afonso, J.C., Begg, G.C., 2009. The composition and evolution of lithospheric mantle: a re-evaluation and its tectonic implications. *J. Petrol.* 50, 1185–1204. <https://doi.org/10.1093/ptrology/egn033>.
- Hammer, P.T., Clowes, R.M., Cook, F.A., van der Velden, A.J., Vasudevan, K., 2010. The Lithoprobe trans-continental lithosphere cross sections: imaging the internal structure of the North American continent. *J. Earth Sci.* 47, 821–857. <https://doi.org/10.1139/E10-036>.
- Hartigan, J.A., 1975. *Clustering Algorithms*, 99th ed. John Wiley & Sons, Inc., USA.
- Hartigan, J.A., Wong, M.A., 1979. Algorithm AS 136: a k-means clustering algorithm. *Appl. Stat.* 28, 100. <https://doi.org/10.2307/2346830>.
- Heaman, L.M., Easton, R.M., Hart, T.R., Hollings, P., Macdonald, C.A., Smyk, M., 2007. Further refinement to the timing of Mesoproterozoic magmatism, Lake Nipigon region, Ontario 1. *Can. J. Earth Sci.* <https://doi.org/10.1139/E06-117>.
- Hieronymus, C.F., Goes, S., 2010. Complex cratonic seismic structure from thermal models of the lithosphere: effects of variations in deep radiogenic heating. *Geophys. J. Int.* 180, 999–1012. <https://doi.org/10.1111/j.1365-246X.2009.04478.x>.
- Hoffman, P.F., 1988. United plates of America, the birth of a craton: Early Proterozoic assembly and growth of Laurentia. *Annu. Rev. Earth Planet. Sci.* 16, 543–603. <https://doi.org/10.1146/annurev.ea.16.050188.002551>.
- Holland, T.J.B., Powell, R., 1998. An internally consistent thermodynamic data set for phases of petrological interest. *J. Metamorph. Geol.* 16, 309–343. <https://doi.org/10.1111/j.1525-1314.1998.00140.x>.
- Hopper, E., Fischer, K.M., 2015. The meaning of midlithospheric discontinuities: a case study in the northern U.S. craton. *Geochim. Geophys. Geosyst.* 16, 4057–4083. <https://doi.org/10.1002/2015GC006030>.
- van Hunen, J., Moyen, J.F., 2012. Archean subduction: fact or fiction? *Annu. Rev. Earth Planet. Sci.* 40, 195–219. <https://doi.org/10.1146/annurev-earth-042711-105255>.
- Hunt, L., Stachel, T., Grütter, H., Armstrong, J., McCandless, T.E., Simonetti, A., Tappe, S., 2012. Small mantle fragments from the Renard kimberlites, Quebec: powerful recorders of mantle lithosphere formation and modification beneath the eastern superior craton. *J. Petrol.* 53, 1597–1635. <https://doi.org/10.1093/ptrology/egs027>.
- Jaupart, C., Mareschal, J.C., Guillou-Frottier, L., Davaille, A., 1998. Heat flow and thickness of the lithosphere in the Canadian Shield. *J. Geophys. Res.*, Solid Earth 103, 15269–15286. <https://doi.org/10.1029/98JB01395>.
- Jordan, T.H., 1978. Composition and development of the continental tectosphere. *Nature* 274, 544–548. <https://doi.org/10.1038/274544a0>.
- Kaufman, L., Rousseeuw, P.J., 1990. *Finding Groups in Data: An Introduction to Cluster Analysis*. John Wiley.
- Lee, C.T., Rudnick, R.L., 1999. Compositionally stratified cratonic lithosphere: petrology and geochemistry of peridotite xenoliths from the Labait tuff cone, Tanzania. In: Gurney, J.J., Richardson, S.R. (Eds.), *International Kimberlite Conference, Red Roof Design*, Cape Town, pp. 503–521.
- Lee, C.T.A., Luffi, P., Chin, E.J., 2011. Building and destroying continental mantle. *Annu. Rev. Earth Planet. Sci.* 39, 59–90. <https://doi.org/10.1146/annurev-earth-040610-133505>.
- Legendre, C.P., Meier, T., Lebedev, S., Friederich, W., Viereck-Götte, L., 2012. A shear wave velocity model of the European upper mantle from automated inversion of seismic shear and surface waveforms. *Geophys. J. Int.* <https://doi.org/10.1111/j.1365-246X.2012.05613.x>.
- Lévy, F., Jaupart, C., 2011. Temperature and rheological properties of the mantle beneath the North American craton from an analysis of heat flux and seismic data. *J. Geophys. Res.* 116, B01408. <https://doi.org/10.1029/2010JB007726>.
- Levy, F., Jaupart, C., Mareschal, J.C., Bienfait, G., Limare, A., 2010. Low heat flux and large variations of lithospheric thickness in the Canadian Shield. *J. Geophys. Res.*, Solid Earth 115, B06404. <https://doi.org/10.1029/2009JB006470>.
- Li, A., Forsyth, D.W., Fischer, K.M., 2003. Shear velocity structure and azimuthal anisotropy beneath eastern North America from Rayleigh wave inversion. *J. Geophys. Res.* 108, 2362. <https://doi.org/10.1029/2002JB002259>.
- Liddell, M., Bastow, I., Rawlinson, N., Darbyshire, F., Gilligan, A., Watson, E., 2018. Precambrian plate tectonics in northern Hudson bay: evidence from P and S-wave seismic tomography and analysis of source side effects in relative arrival-time datasets. *J. Geophys. Res.*, Solid Earth 123, 5690–5709. <https://doi.org/10.1029/2018JB015473>.
- Mareschal, J., Jaupart, C., 2004. Variations of surface heat flow and lithospheric thermal structure beneath the North American craton. *Earth Planet. Sci. Lett.* 223, 65–77. <https://doi.org/10.1016/j.epsl.2004.04.002>.
- Masters, G., Woodhouse, J., Freeman, G., 2011. Mineos v1.0.2.
- Miller, M.S., Eaton, D.W., 2010. Formation of cratonic mantle keels by arc accretion: evidence from S receiver functions. *Geophys. Res. Lett.* 37. <https://doi.org/10.1029/2010GL044366>.
- Musacchio, G., White, D.J., Asudeh, I., Thomson, C.J., 2004. Lithospheric structure and composition of the Archean western Superior Province from seismic refraction/wide-angle reflection and gravity modeling. *J. Geophys. Res.* 109, B03304. <https://doi.org/10.1029/2003JB002427>.
- O'Reilly, S.Y., Griffin, W.L., 2010. The continental lithosphere-asthenosphere boundary: can we sample it? *Lithos* 120, 1–13. <https://doi.org/10.1016/j.lithos.2010.03.016>.
- Pearson, D., Canil, D., Shirey, S., 2003. Mantle samples included in volcanic rocks: xenoliths and diamonds. In: *Treatise on Geochemistry*, vol. 2, pp. 171–275.
- Percival, J.A., Sanborn-Barrie, M., Skulski, T., Stott, G.M., Helmsstaedt, H., White, D.J., 2006. Tectonic evolution of the western Superior Province from NATMAP and Lithoprobe studies. *Can. J. Earth Sci.* 43, 1085–1117. <https://doi.org/10.1139/E06-062>.
- Percival, J.A., Skulski, T., Sanborn-Barrie, M., Stott, G.M., Leclair, A.D., Corkery, M.T., Boily, M., 2012. *Geology and tectonic evolution of the Superior Province, Canada. In: Tectonic Styles in Canada: The Lithoprobe Perspective*, pp. 321–378.
- Perry, H.K.C., Jaupart, C., Mareschal, J.C., Bienfait, G., 2006a. Crustal heat production in the Superior Province, Canadian Shield, and in North America inferred from heat flow data. *J. Geophys. Res.* 111, B04401. <https://doi.org/10.1029/2005JB003893>.
- Perry, H.K.C., Jaupart, C., Mareschal, J.C., Shapiro, N.M., 2006b. Upper mantle velocity-temperature conversion and composition determined from seismic refraction and heat flow. *J. Geophys. Res.*, Solid Earth 111. <https://doi.org/10.1029/2005JB003921>.
- Petrescu, L., Bastow, I.D., Darbyshire, F.A., Gilligan, A., Bodin, T., Menke, W., Levin, V., 2016. Three billion years of crustal evolution in eastern Canada: constraints from receiver functions. *J. Geophys. Res.*, Solid Earth 121, 788–811. <https://doi.org/10.1002/2015JB012348>.
- Petrescu, L., Darbyshire, F., Bastow, I., Totten, E., Gilligan, A., 2017. Seismic anisotropy of Precambrian lithosphere: insights from Rayleigh wave tomography of the eastern Superior Craton. *J. Geophys. Res.*, Solid Earth 122, 3754–3775. <https://doi.org/10.1002/2016JB013599>.
- Porritt, R.W., Miller, M.S., Darbyshire, F.A., 2015. Lithospheric architecture beneath Hudson Bay. *Geochim. Geophys. Geosyst.* 16, 2262–2275. <https://doi.org/10.1002/2015GC005845>.
- Rousseeuw, P.J., 1987. Silhouettes: a graphical aid to the interpretation and validation of cluster analysis. *J. Comput. Appl. Math.* 20, 53–65. [https://doi.org/10.1016/0377-0427\(87\)90125-7](https://doi.org/10.1016/0377-0427(87)90125-7).
- Schutt, D.L., Leshner, C.E., 2006. Effects of melt depletion on the density and seismic velocity of garnet and spinel lherzolite. *J. Geophys. Res.* 111, 5401. <https://doi.org/10.1029/2003JB002950>.
- Scully, K.R., Canil, D., Schulze, D.J., 2004. The lithospheric mantle of the Archean Superior Province as imaged by garnet xenocryst geochemistry. *Chem. Geol.* 207, 189–221. <https://doi.org/10.1016/j.chemgeo.2004.03.001>.
- Selway, K., Yi, J., Karato, S.I., 2014. Water content of the Tanzanian lithosphere from magnetotelluric data: implications for cratonic growth and stability. *Earth Planet. Sci. Lett.* 388, 175–186. <https://doi.org/10.1016/j.epsl.2013.11.024>.
- Shapiro, N.M., Ritzwoller, M.H., Mareschal, J.C., Jaupart, C., 2004. Lithospheric structure of the Canadian Shield inferred from inversion of surface-wave dispersion with thermodynamic *a priori* constraints. *Geol. Soc. (Lond.) Spec. Publ.* 239, 175–194. <https://doi.org/10.1144/GSL.SP.2004.239.01.12>.
- Shay, J., Tréhu, A., 1993. Crustal structure of the central graben of the Midcontinent Rift beneath Lake Superior. *Tectonophysics* 225, 301–335. [https://doi.org/10.1016/0040-1951\(93\)90303-2](https://doi.org/10.1016/0040-1951(93)90303-2).
- Sleep, N.H., 2005. Evolution of the continental lithosphere. *Annu. Rev. Earth Planet. Sci.* 33, 369–393. <https://doi.org/10.1146/annurev.earth.33.092203.122643>.
- Thomas, W.A., 1991. The Appalachian-Ouachita rifted margin of southeastern North America. *Geol. Soc. Am. Bull.* 103, 415–431. [https://doi.org/10.1130/0016-7606\(1991\)103<0415:TAORMO>2.3.CO;2](https://doi.org/10.1130/0016-7606(1991)103<0415:TAORMO>2.3.CO;2).
- Thompson, D.A., Kendall, J., Helffrich, G.R., Bastow, I.D., Wookey, J., Snyder, D.B., 2015. CAN HK: an a priori crustal model for the Canadian Shield. *Seismol. Res. Lett.* 86, 1374–1382. <https://doi.org/10.1785/0220150015>.

- Thurston, P.C., 1991. *Geology of Ontario*, 4 ed. Ontario Ministry of Northern Development and Mines.
- Wang, H., van Hunen, J., Pearson, D.G., Allen, M.B., 2014. Craton stability and longevity: the roles of composition-dependent rheology and buoyancy. *Earth Planet. Sci. Lett.* 391, 224–233. <https://doi.org/10.1016/j.epsl.2014.01.038>.
- Weller, O., Copley, A., Miller, W., Palin, R., Dyck, B., 2019. The relationship between mantle potential temperature and oceanic lithosphere buoyancy. *Earth Planet. Sci. Lett.* 518, 86–99. <https://doi.org/10.1016/j.epsl.2019.05.005>.
- White, D.J., Forsyth, D.A., Asudeh, I., Carr, S.D., Wu, H., Easton, R.M., Mereu, R.F., 2000. A seismic-based cross-section of the Grenville Orogen in southern Ontario and western Quebec. *Can. J. Earth Sci.* 37, 183–192. <https://doi.org/10.1139/e99-094>.
- Whitmeyer, S.J., Karlstrom, K.E., 2007. Tectonic model for the Proterozoic growth of North America. *Geosphere* 3, 220–259. <https://doi.org/10.1130/GES00055.1>.
- Winardhi, S., Mereu, R.F., 1997. Crustal velocity structure of the Superior and Grenville provinces of the southeastern Canadian Shield. *Can. J. Earth Sci.* 34, 1167–1184. <https://doi.org/10.1139/e17-094>.
- Wyman, D.A., Hollings, P., Conceição, R.V., 2014. Geochemistry and radiogenic isotope characteristics of xenoliths in Archean diamondiferous lamprophyres: implications for the Superior Province cratonic keel. *Lithos* 233, 111–130. <https://doi.org/10.1016/j.lithos.2015.02.018>.
- Yuan, H., Levin, V., 2014. Stratified seismic anisotropy and the lithosphere–asthenosphere boundary beneath eastern North America. *J. Geophys. Res., Solid Earth* 119, 3096–3114. <https://doi.org/10.1002/2013JB010785>.
- Yuan, H., Romanowicz, B., 2010. Lithospheric layering in the North American craton. *Nature* 466, 1063–1068. <https://doi.org/10.1038/nature09332>.
- Zhang, H., van der Lee, S., Wolin, E., Bollmann, T.A., Revenaugh, J., Wiens, D.A., Frederiksen, A.W., Darbyshire, F.A., Aleqabi, G.I., Wysession, M.E., Stein, S., Jurdy, D.M., 2016. Distinct crustal structure of the North American Midcontinent rift from P wave receiver functions. *J. Geophys. Res., Solid Earth* 121, 8136–8153. <https://doi.org/10.1002/2016JB013244>.